Supporting Information

Size- and Composition-Dependent Radio Frequency Magnetic Permeability of Iron Oxide Nanocrystals

Hongseok Yun[1], Xiyu Liu[2], Taejong Paik[1], Duraivelan Palanisamy[2], Jungkwun Kim[3], William D. Vogel[4], Arthur J. Viescas[4], Jun Chen[2,†], Georgia C. Papaefthymiou[4], James M. Kikkawa[5], Mark G. Allen[3], Christopher B. Murray[1,2,]*

[1]*Department of Chemistry, University of Pennsylvania, Philadelphia, Pennsylvania 19104, United States*

[2]*Department of Materials Science and Engineering, University of Pennsylvania, Philadelphia, Pennsylvania 19104, United States*
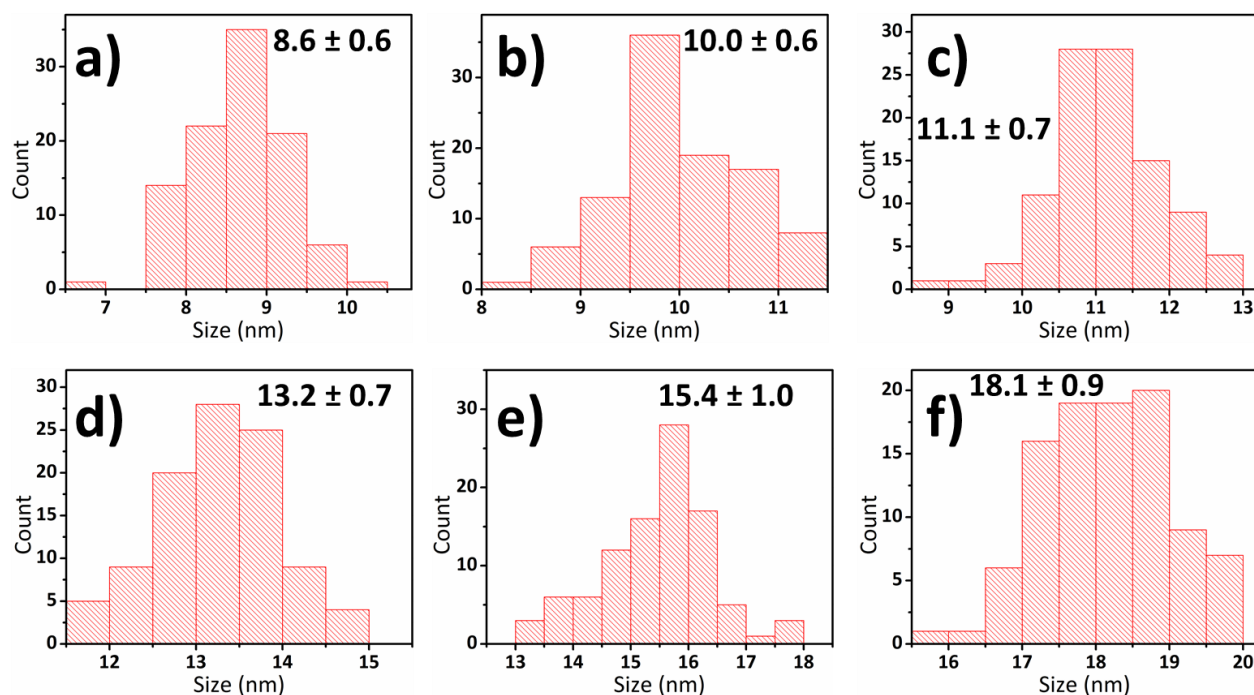
[3]*Department of Electrical and Systems Engineering, University of Pennsylvania, Philadelphia, Pennsylvania 19104, United States*

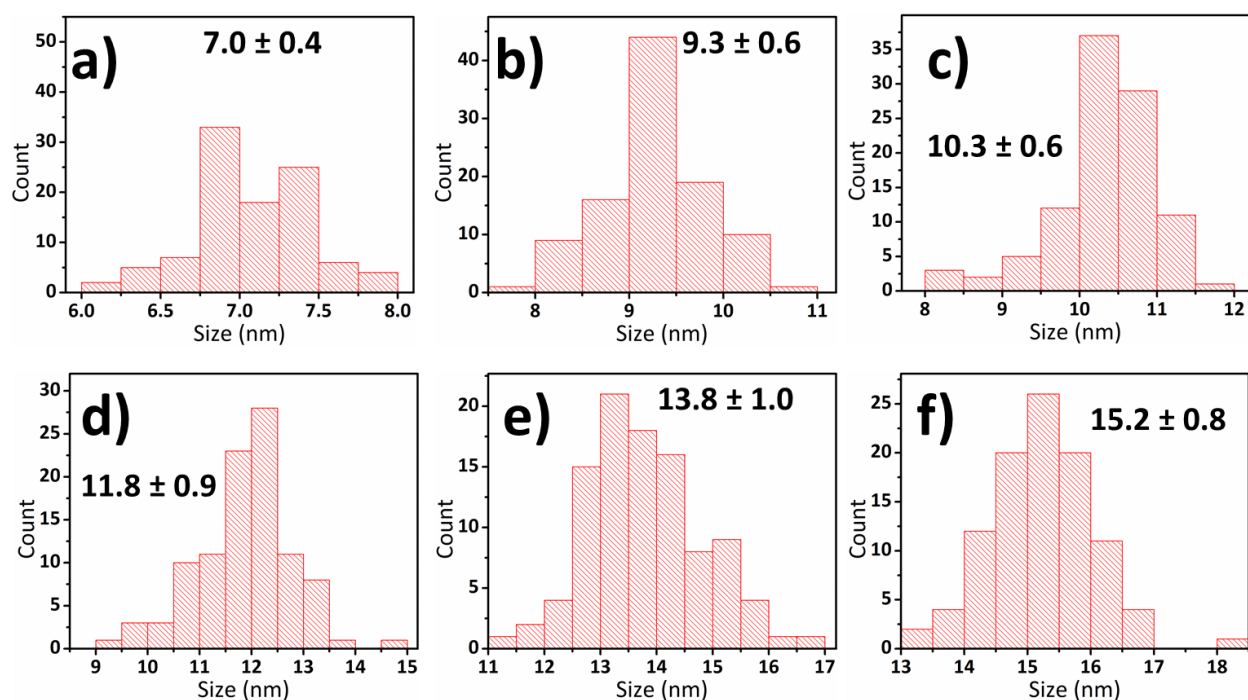[4]*Department of Physics, Villanova University, Villanova, Pennsylvania 19085, United States*

[5]*Department of Physics and Astronomy, University of Pennsylvania, Philadelphia, Pennsylvania 19104, United States*

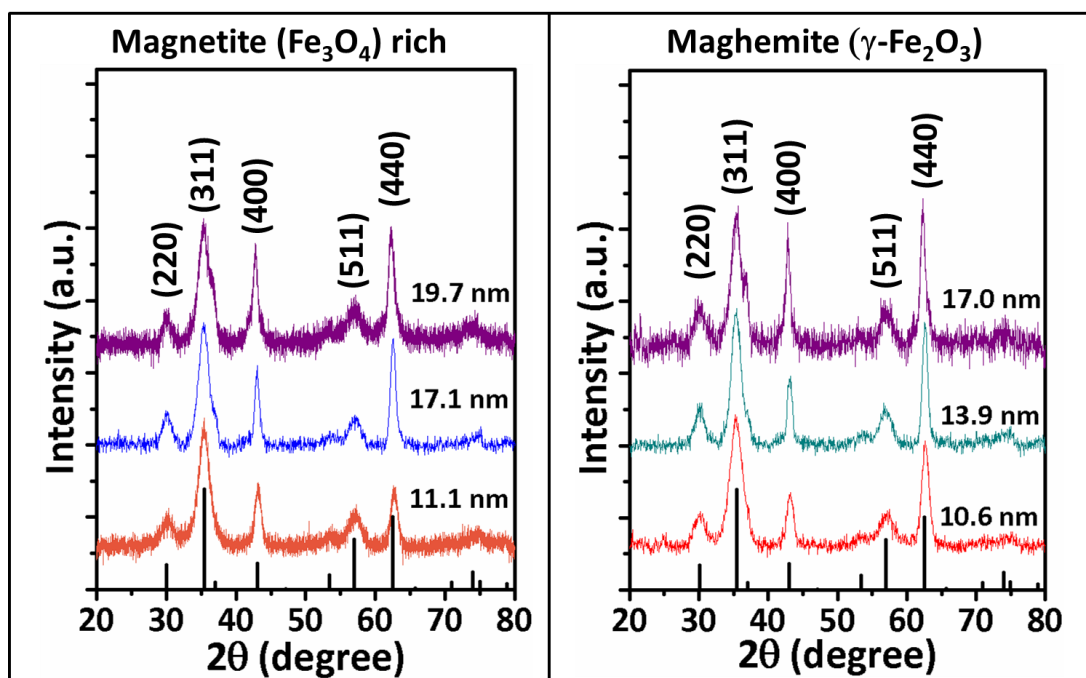[*]*Address correspondence to cbmurray@sas.upenn.edu*

[†]*Present Addresses: HGST, a Western Digital company, 3403 Yerba Buena Road, San Jose, California 95135, United States*
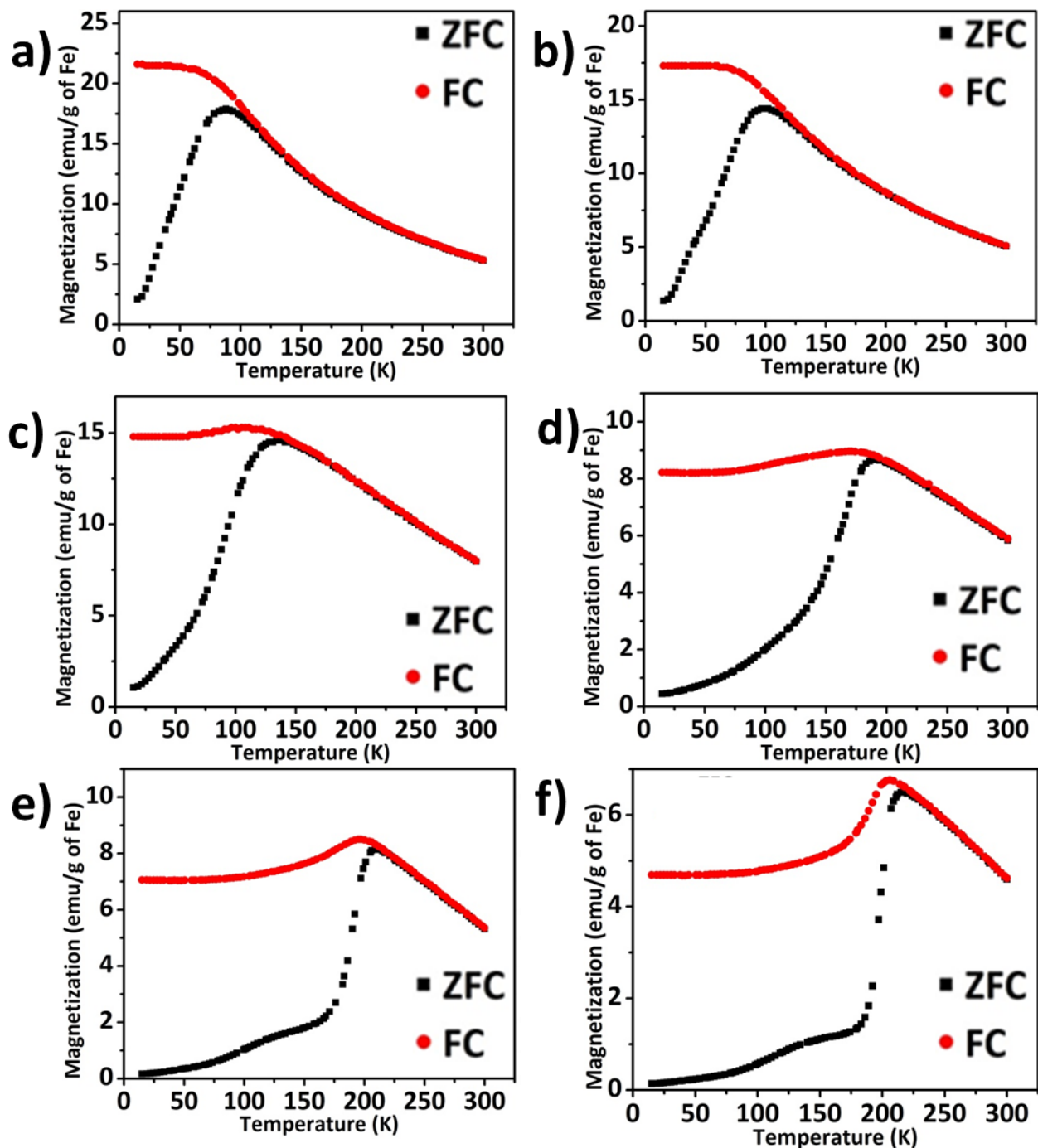
Figure S1. Histograms of NC sizes a) 10.2 nm, b) 11.1 nm, c) 12.8 nm, d) 14.9 nm, e) 17.1 nm, and f) 19.7 nm as-synthesized iron oxide nanocrystals from TEM images. The numbers in the figures are the average size and standard deviation based on the TEM images.
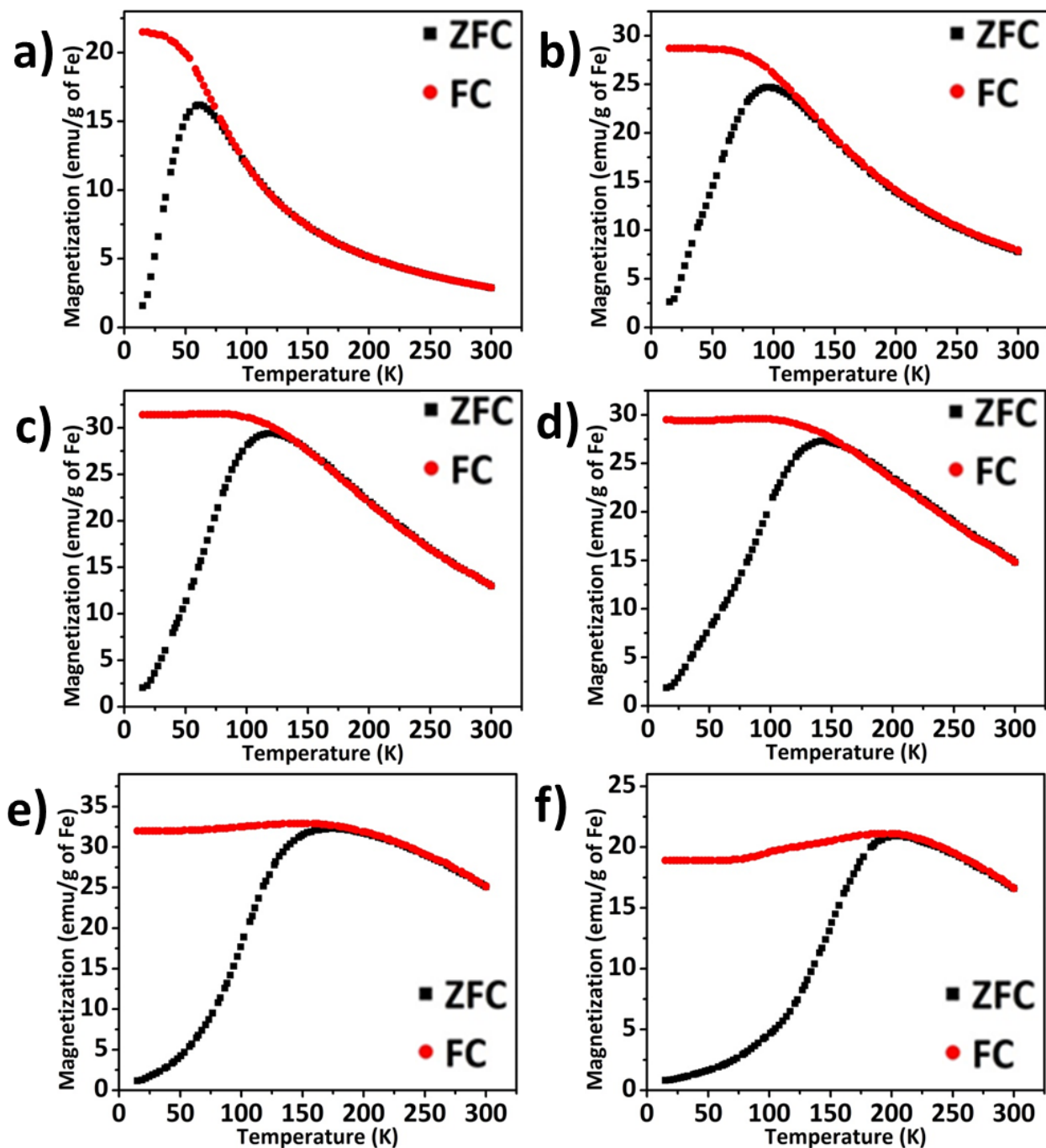

Figure S2. Histograms of NC sizes a) 8.6 nm, b) 10.6 nm, c) 12.3 nm, d) 13.9 nm, e) 15.6 nm, and f) 17.0 nm as-synthesized iron oxide nanocrystals from TEM images. The numbers in the figures are the averaged size and standard deviation based on the TEM images.
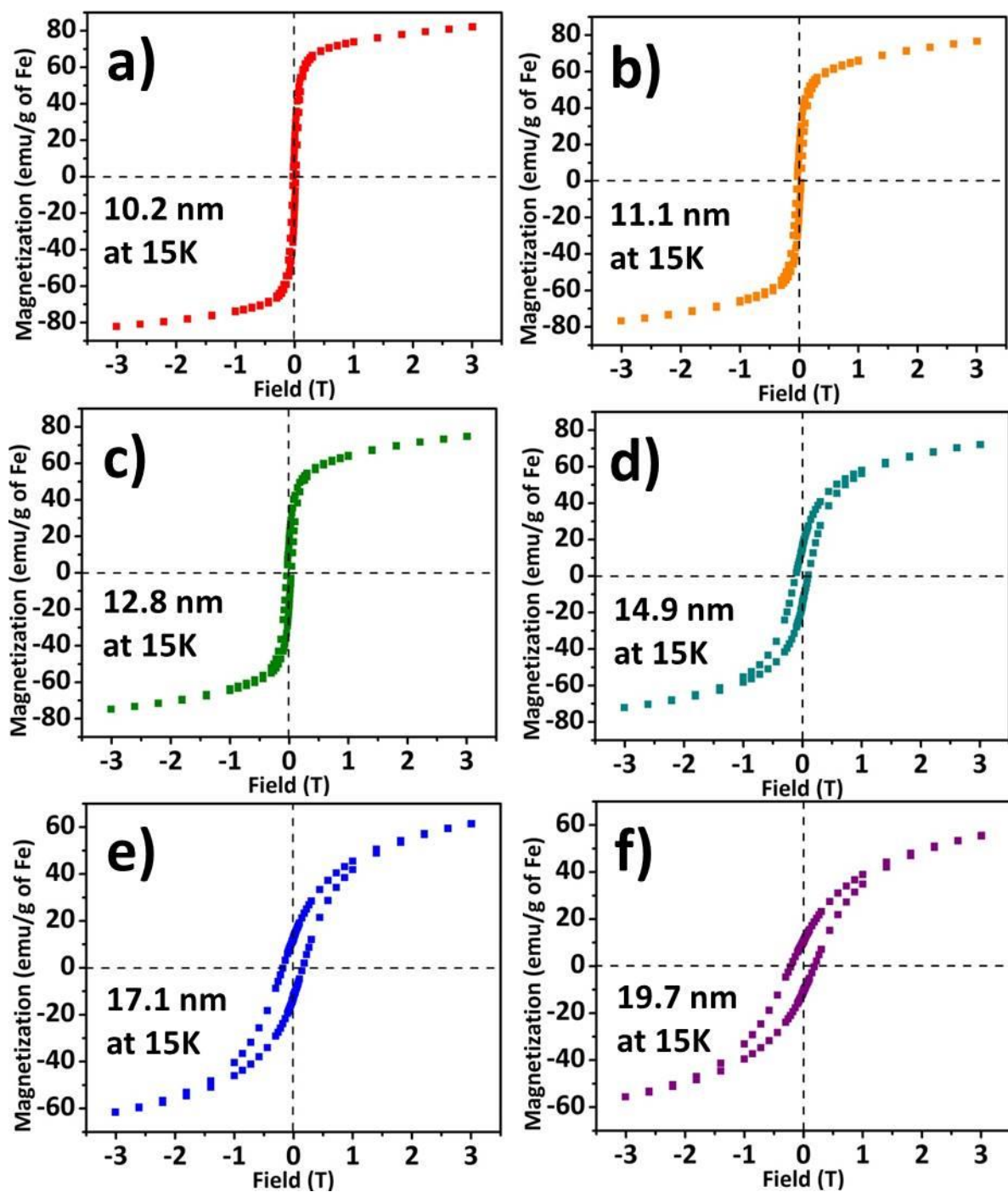
Figure S3. Wide angle x-ray scattering data of magnetite-rich (left) and maghemite iron oxide nanocrystals (right).

Figure S4. Field Cooling (FC, red circles) and Zero Field Cooling (ZFC, black squares) curves of a) 10.2 nm, b) 11.1 nm, c) 12.8 nm, d) 14.9 nm, e) 17.1 nm, and f) 19.7 nm magnetite-rich iron oxide nanocrystals.
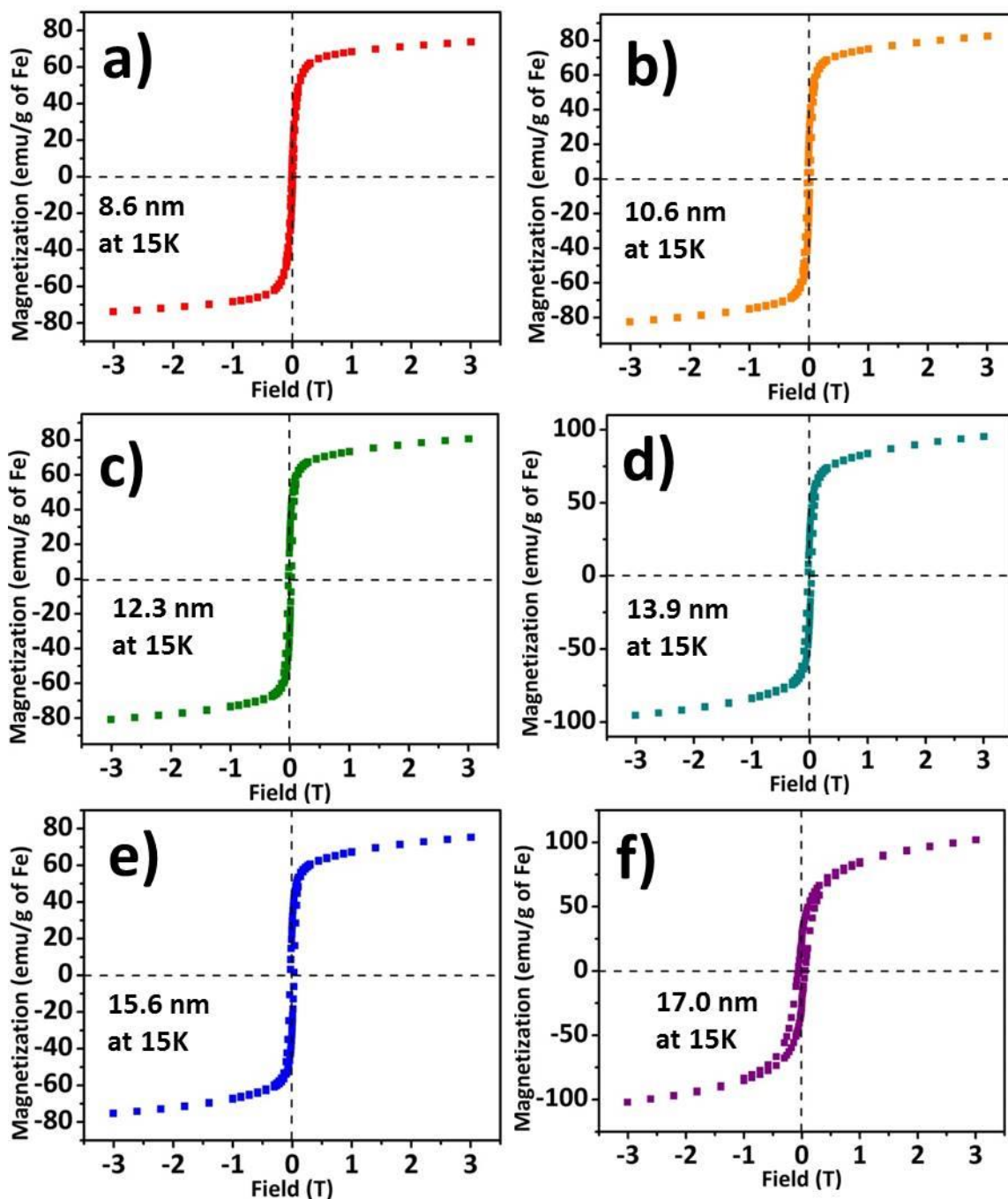
Figure S5. Field Cooling (FC, red circles) and Zero Field Cooling (ZFC, black squares) curves of a) 8.6 nm, b) 10.6 nm, c) 12.3 nm, d) 13.9 nm, e) 15.6 nm, and f) 17.0 nm maghemite iron oxide nanocrystals.
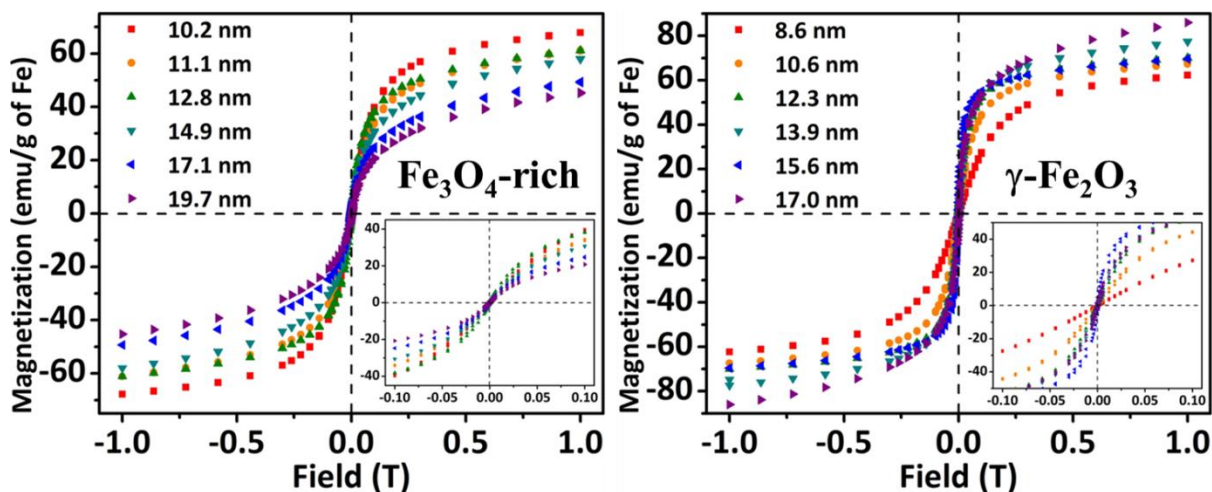
Figure S6. Hysteresis curves of a) 10.2 nm, b) 11.1 nm, c) 12.8 nm, d) 14.9 nm, e) 17.1 nm, and f) 19.7 nm magnetite-rich iron oxide NCs at 15 K.
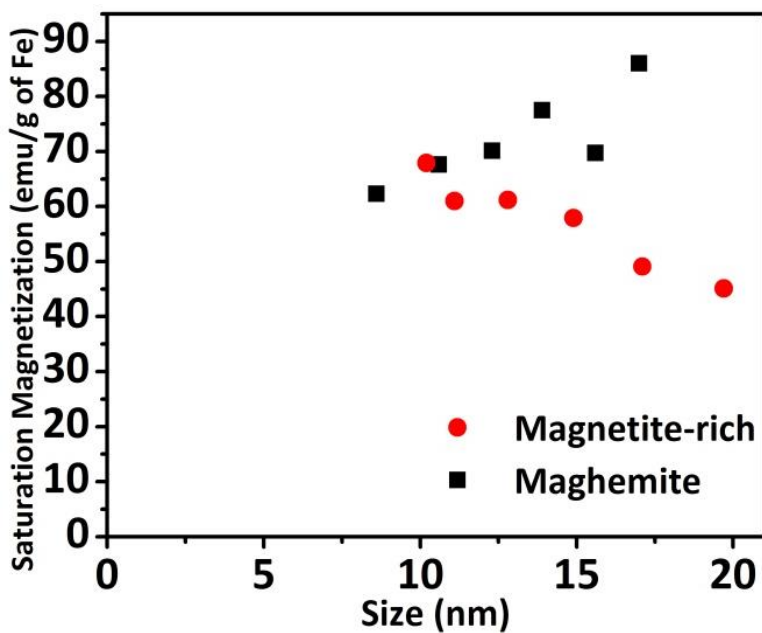
Figure S7. Hysteresis curves of a) 8.6 nm, b) 10.6 nm, c) 12.3 nm, d) 13.9 nm, e) 15.6 nm, and f) 17.0 nm maghemite iron oxide NCs at 15 K.

Figure S8. Hysteresis curves of a) magnetite-rich iron oxide NCs and b) maghemite iron oxide NCs at 300 K. Insets are zoomed -up images of each at low field.
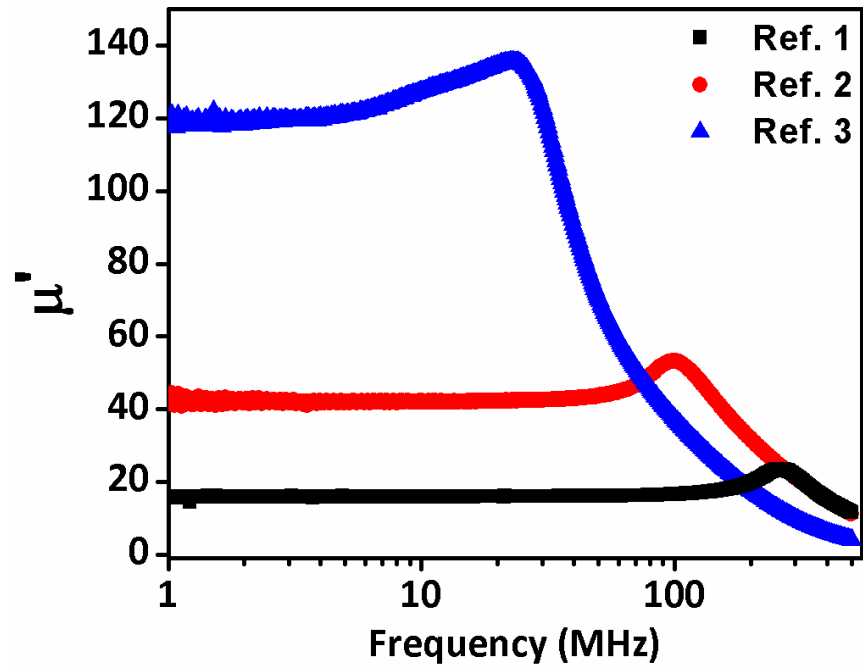

Figure S9. Saturation magnetization value of magnetite-rich (red circle) and maghemite (black square) iron oxide NCs at 300 K.

Frequency dependence of the real and imaginary parts of the magnetic susceptibility

$$\chi' = \chi_\infty + \frac{\chi_0 - \chi_\infty}{1 + (\omega \cdot \tau)^2} \quad \text{and} \quad \chi'' = \frac{(\chi_0 - \chi_\infty) \cdot \omega \cdot \tau}{1 + (\omega \cdot \tau)^2} \qquad \text{SI (1)}$$

Here χ_0 is the initial static susceptibility at zero frequency (initial slopes in Fig. S8 insets),

χ_∞ is the susceptibility at the highest frequency, $\omega = 2\pi f$ and τ is the relaxation time.[1] At

temperatures above T_b the particles become superparamagnetic and the relaxation time $\tau \rightarrow \tau_0$

with increasing temperature; the frequency dependence of the complex susceptibility then

becomes characteristic of the corresponding bulk material. Thus, according to Eq. SI(1) the real

part of the AC susceptibility is expected to exhibit an initial maximum plateau at low frequencies,

corresponding to χ_0, when the magnetization has time to respond and follow the applied AC

field; it will then start to decrease as the frequency increases, while the imaginary part of the

susceptibility will exhibit a characteristic maximum at a certain frequency. This behavior is

reflected in our experimental data of the relative permeability, μ, of the maghemite samples of
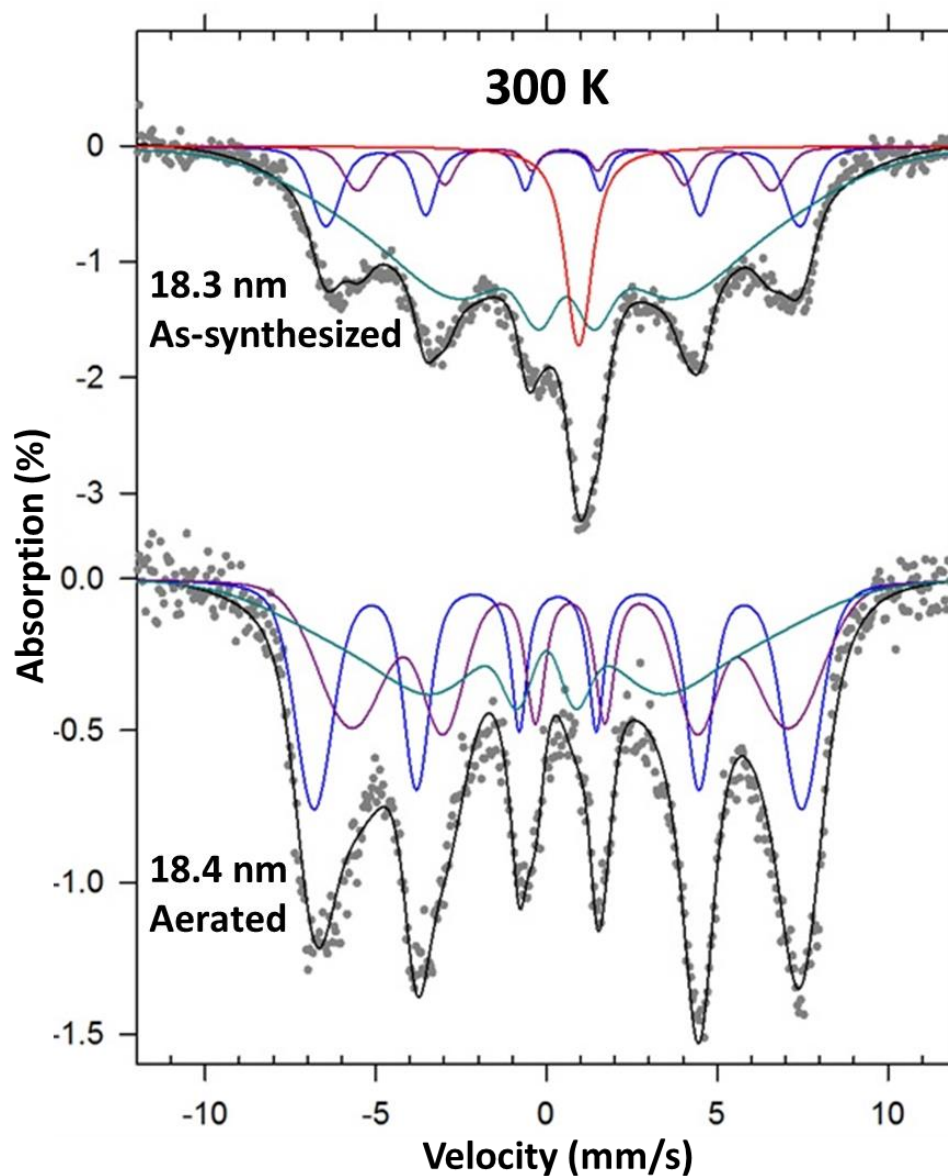
Figures 4 and 5, where $\mu_r = 1 + \chi$.

Figure S10. Real part of permeability of commercially available ferrite toroid.

Provided relative permeability of references
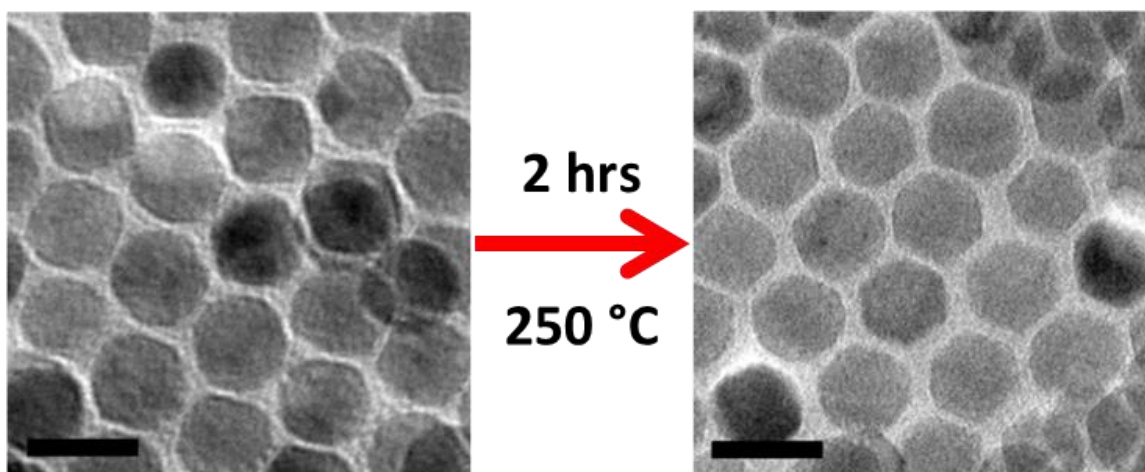Ref#1: 20
Ref#2: 40
Ref#3: 120

Figure S11. Mössbauer spectra of as-synthesized and aerated NC samples at 300 K as indicated. The experimental points are least square fitted (black line) to a superposition of theoretical spectra of tetrahedral Fe^{3+} (blue), octahedral $Fe^{2.5+}$ (purple) sites, interfacial $Fe_{1-x}O/Fe_3O_4$ (red) and intermediate relaxation (pale green) sites (Table S1).
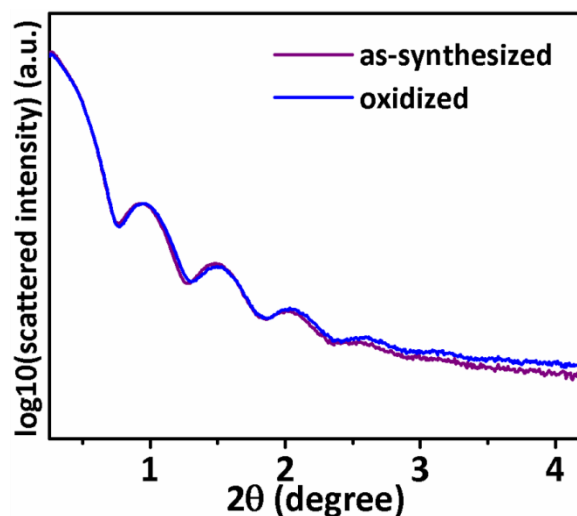
Table S1. Mössbauer hyperfine parameters derived from spectral fits shown in Fig. S11. δ, Isomer shift relative to metallic iron at RT, ΔE_Q, Quadrupole splitting, H_{hf}, Hyperfine magnetic field.

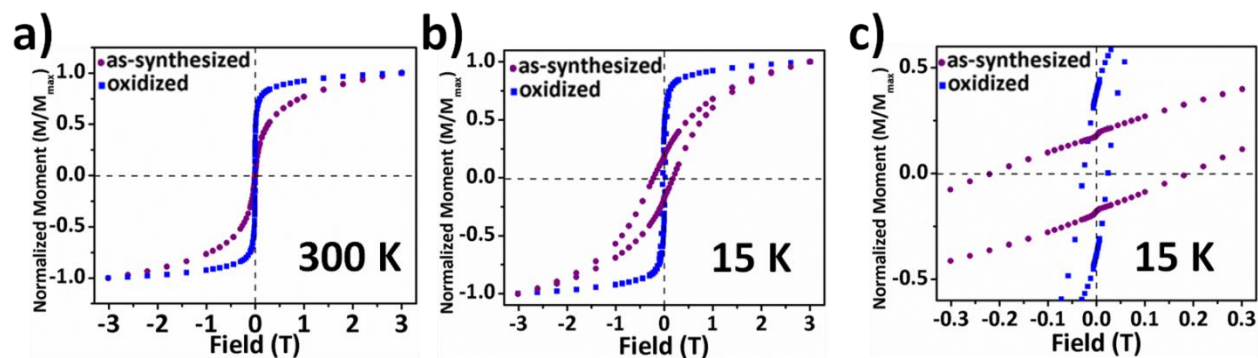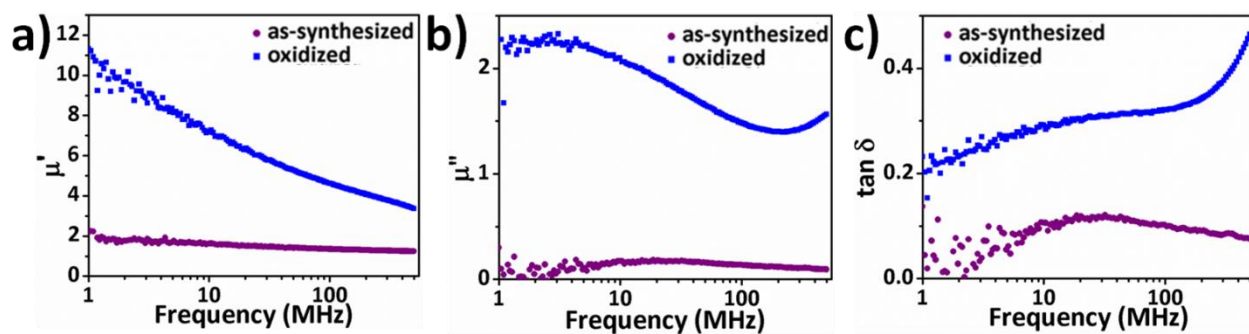| Sample	Size (by SAXS)	T (K)	Site	δ (mm/s)	ΔE_Q (mm/s)	H_{hf}(T)	Area (%)
As-synthesized Iron Oxide NCs	18.3 nm	300	Interfacial*	0.94	-	-	9.1
			Fe^{3+} (A)	0.47	-	42.9	13.7
			$Fe^{2.5+}$ [B]	0.53	-	27.5	7.6
			IR	0.58	-	-	69.6
After heating at 250 °C for 2 hours	18.4 nm	300	Fe^{3+} (A)	0.33	-	44.2	32.3
			$Fe^{2.5+}$ [B]	0.69	-	39.6	34.4
			IR	0	-	-	33.3

*$Fe_{1-x}O/Fe_3O_4$

Figure S12. TEM images of 18.3 nm iron oxide NCs before (left) and after (right) oxidation process. These TEM images show that there is almost no change neither in morphology nor in size of NCs after oxidation process at 250 °C. The scale bar is 20 nm.

Figure S13. SAXS curves of as-synthesized iron oxide NCs and iron oxide NCs which are aged at 250 °C for 2 hours.
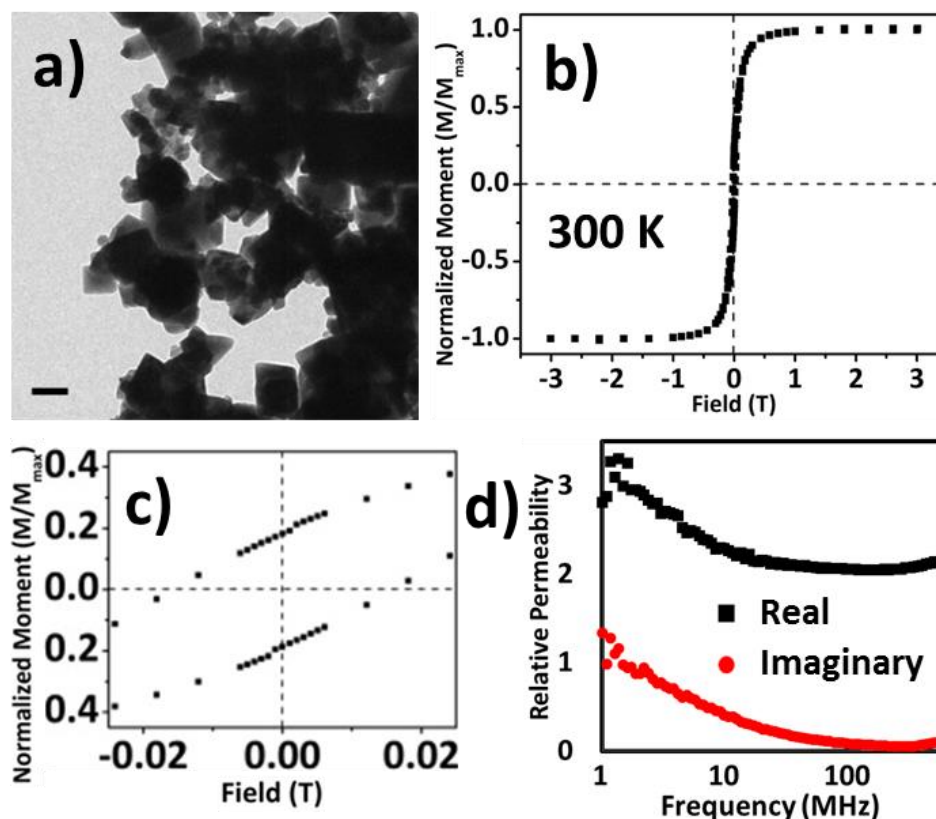

Figure S14. Magnetic hysteresis curves of 18.3 nm iron oxide nanocrystals before and after aeration process. a) 300 K hysteresis curves, b) 15 K hysteresis curves, and c) zoomed up 15 K hysteresis curves from 0.3 T to -0.3 T of as-synthesized 18.3 nm iron oxide nanocrystals (purple) and oxidized iron oxide nanocrystals (blue).

Figure S15. a) Real part of permeability, b) imaginary part of permeability, and c) tangent loss of as-synthesized 18.3 nm iron oxide nanocrystals (purple) and oxidized iron oxide nanocrystals (blue).

Figure S16. a) TEM image, b) hysteresis curve at 300 K, c) the expanded image of the hysteresis curve at 300 K, and d) the relative permeability of commercially available iron oxide (Fe_3O_4) powder, particle size <5 μm. The scale bar in the TEM image is 100 nm.

For comparison, commercially available ferromagnetic iron oxide powder is tested as well. As can be seen in figure S16, this ferromagnetic iron oxide powder is suffered by high imaginary part of permeability at relatively low frequency (< 10 MHz) and low real part of permeability at relatively high frequency (> 10 MHz) range. In addition, our NCs are superior to the ferromagnetic iron oxide powder in that iron oxide NCs are dispersible in volatile solvent, which makes them readily available for solution based deposition processes.

Reference

1.   Lucchini, M. A.; Riani, P.; Canepa, F. Quantitative Analysis of the A.C. Susceptibility of Core–Shell Nanoparticles. *J. Nanopart. Res.* 2013, 15. 1601.